

# Efficient Parallel Algorithms for Inpainting-Based Representations of 4K Images - Part I: Homogeneous Diffusion Inpainting \*

Niklas Kämper <sup>†</sup>, Vassillen Chizhov<sup>†</sup>, and Joachim Weickert<sup>†</sup>

**Abstract.** In recent years inpainting-based compression methods have been shown to be a viable alternative to classical codecs such as JPEG and JPEG2000. Unlike transform-based codecs, which store coefficients in the transform domain, inpainting-based approaches store a small subset of the original image pixels and reconstruct the image from those by using a suitable inpainting operator. A good candidate for such an inpainting operator is homogeneous diffusion inpainting, as it is simple, theoretically well-motivated, and can achieve good reconstruction quality for optimized data. However, a major challenge has been to design fast solvers for homogeneous diffusion inpainting that scale to 4K image resolution ( $3840 \times 2160$  pixels) and are real-time capable. We overcome this with a careful adaptation and fusion of two of the most efficient concepts from numerical analysis: multigrid and domain decomposition. Our domain decomposition algorithm efficiently utilizes GPU parallelism by solving inpainting problems on small overlapping blocks. Unlike simple block decomposition strategies such as the ones in JPEG, our approach yields block artifact-free reconstructions. Furthermore, embedding domain decomposition in a full multigrid scheme provides global interactions and allows us to achieve optimal convergence by reducing both low- and high-frequency errors at the same rate. We are able to achieve 4K color image reconstruction at more than 60 frames per second even from very sparse data - something which has been previously unfeasible.

**Key words.** Inpainting, Homogeneous Diffusion, Domain Decomposition, Multigrid, GPU

**MSC codes.** 65N22, 65N55, 65D18, 68U10, 94A08

**1. Introduction.** The classical image inpainting task deals with the reconstruction of missing parts of partially corrupted images [5, 9, 23, 30, 52, 61, 63]. However, it has also been successfully used in image compression methods [1, 6, 16, 21, 26, 28, 39, 49, 56, 57, 59, 62, 64, 72, 73, 76] as an alternative to classical transform-based approaches. In the encoding phase, these methods store a small optimized subset of the image data. The decoding phase then consists of reconstructing the missing parts of the image from the stored data by an inpainting process. Sparse nonlinear diffusion-based inpainting for image compression was introduced by Galić et al. [25] in 2005, later improved by Schmaltz et al. [62], and extended to color images by Peter et al. [57]. They showed that inpainting-based methods can qualitatively outperform the widely used JPEG [55] and JPEG2000 [67] for images with small to medium amounts of texture.

Surprisingly, already with simple linear homogeneous diffusion [36] one can obtain very good inpainting results, if the locations as well as the values of the known pixels are carefully

---

\*Part of this work has been published as a conference paper [42].

**Funding:** This work has received funding from the European Research Council (ERC) under the European Union's Horizon 2020 research and innovation programme (grant agreement no. 741215, ERC Advanced Grant INCOVID)

<sup>†</sup>Mathematical Image Analysis Group, Faculty of Mathematics and Computer Science, Campus E1.7, Saarland University, 66041 Saarbrücken, Germany (kaemper@mia.uni-saarland.de, chizhov@mia.uni-saarland.de, weickert@mia.uni-saarland.de)

optimized [7, 10, 13, 18, 33, 51]. For piecewise constant images, such as cartoon images, depth maps or flow fields, one can achieve state-of-the-art results [28, 34, 48, 50], and some of these methods [37, 38] even outperform HEVC [66]. Its advantage, in contrast to nonlinear inpainting methods, is its simplicity, since it is parameter-free and its finite difference discretization yields a sparse pentadiagonal linear system of size  $N \times N$ , where  $N$  is the number of pixels in the image.

However, computing the solution of such large linear systems can be quite time-consuming. Nowadays, 4K color images of size  $3840 \times 2160$  pixels are a standard, resulting in systems with approximately 8 million equations and the same number of unknowns for each color channel, and either 30 or 60 frames per second are usually required for video playback. Thus, it would be desirable to achieve real-time decoding for 4K color images with at least 30 or 60 frames per second. Even though there has been substantial research to accelerate inpainting-based compression [2, 3, 19, 35, 40, 46, 50, 58], achieving 4K color inpainting at 60 frames per second for very sparse data has been previously unfeasible. Current approaches are at least one order of magnitude slower. However, most of their numerical solvers have been tailored towards sequential or mildly parallel architectures, such as CPUs. They do not exploit the potential of highly parallel architectures such as GPUs, which are widely available these days.

We exploit this potential with our approach by carefully adapting and merging two of the most efficient concepts from numerical analysis, that have been rarely used in image analysis so far: domain decomposition [22, 68] and multigrid [12, 14, 31, 69, 71]. Domain decomposition methods [22, 68] decompose the image domain into multiple subdomains and solve linear systems on each subdomain in parallel, instead of working directly on the large global linear system.

They benefit from highly parallel architectures, due to the decomposition into multiple small subdomains. By providing mechanisms for communication across subdomain boundaries and iterating this process, one can achieve convergence to the solution of the global problem. This results in a reconstruction without any artifacts at the block boundaries, unlike simple block decompositions such as in JPEG. However, while domain decomposition methods are very efficient at decreasing high frequency modes of the error, they are not able to decrease the lower frequencies at the same rate. Multigrid methods [12, 14, 31, 69, 71] allow for a more efficient interaction between subdomains that are far apart. They construct a multiresolution representation of the problem and decimate the different frequencies of the error at the different resolutions. This results in a similar rate of decrease of both the low- and high-frequency components of the error, and also leads to an optimal linear scaling behavior.

**1.1. Our Contribution.** The goal of our paper is to develop a fast solver for homogeneous diffusion inpainting, in order to make 4K image and video compression with homogeneous diffusion practical. We do so by devising a new powerful algorithmic approach that fuses ideas from two very efficient concepts in numerical analysis: full multigrid [12, 14, 31, 69, 71] and domain decomposition methods [22, 68].

In our conference paper contribution on real-time 4K image inpainting [42] we have successfully employed a multilevel domain decomposition method to solve the homogeneous diffusion inpainting equation in real-time for 4K color images with 30 frames per second on a contemporary GPU. We have shown that domain decomposition methods are well suited for

homogeneous diffusion inpainting, because in practice the influence area of each known pixel is localized.

We expand on our conference paper by extending our multilevel optimized restricted additive Schwarz (ORAS) method for homogeneous diffusion inpainting to a full multigrid approach with even more resolution layers. We improve the visual quality of our multigrid approach by a new initial downsampling method that adapts better to the image and the inpainting data. The full multigrid ORAS solver is more robust with respect to the mask density, which enables real-time performance even for very low densities. Furthermore, we are able to reach the current standard in video coding of 60 frames per second at 4K resolution if at least 2% of the image data is known.

This paper is the first part of a companion paper on homogeneous diffusion inpainting. In the second part, we focus on the encoding, which consists of optimizing the inpainting data.

**1.2. Related Work.** In the following we discuss prior work on accelerating diffusion-based inpainting. In contrast to previous methods, we exploit the highly parallel nature of current GPUs and do not rely on any sort of temporal coherence of subsequent video frames. We integrate multigrid ideas, but complement them with a highly parallel domain decomposition method.

*Domain Decomposition in Image Processing.* While domain decomposition methods have not been used for sparse image inpainting, there exist a few domain decomposition approaches for image processing tasks, such as denoising [17, 44, 75], optic flow computation [45] or deblurring [74].

*Multigrid Methods.* Multigrid methods [12, 14, 31, 69, 71] belong to the most efficient solvers for linear and nonlinear systems. They solve problems on multiple resolutions simultaneously, in order to achieve uniform convergence for both high- and low-frequency components of the error. Both Köstler et al. [46] and Mainberger et al. [50] use them for homogeneous diffusion inpainting on mildly parallel architectures such as multicore CPUs [50] or the *Playstation 3* [46]. For the smoothing operations on each level of the multigrid method, both approaches use a simple Gauss-Seidel iteration [60]. Köstler et al. [46] also considered nonlinear anisotropic diffusion with a coarse-to-fine multilevel method. While our approach also employs a (full) multigrid method, we improve the downsampling by adapting it to the inpainting operator, and we use a more sophisticated smoother, i.e. domain decomposition, that better utilizes GPU parallelism.

*Green's Functions.* Another approach for accelerated inpainting goes back to Hoffmann et al. [35]. It is based on discrete Green's functions [4, 8, 20]. They can be used to decompose the inpainting problem into pixel-wise contributions from which the reconstruction can be assembled as a linear combination. This leads to an alternative system matrix of size  $|K| \times |K|$  where  $|K|$  is the number of known pixels, which determines the coefficients in the linear combination. This approach has the advantage that its runtime depends only on the number of mask pixels instead of the overall number of pixels. For very sparse inpainting data it can, thus, outperform multigrid methods. However, its system matrix is dense, and its size grows quadratically with the number of mask pixels. Thus, for 4K images and typical mask densities between 1% and 5% this approach is infeasible due to memory and runtime constraints. Kalmoun and Nasser's [40] approach is based on continuous Green's functions

used in the method of fundamental solutions [43, 47]. They use a GMRES [60] solver with a fast multipole method [29]. The closed-form of the Green’s functions coupled with the fast multipole method allow them to avoid storing the system matrix circumventing the memory constraints. Nevertheless, the inpaintings are still not real-time even at low resolutions such as  $256 \times 256$ .

**Finite Elements.** Chizhov and Weickert [19] replace the standard finite difference discretization of homogeneous diffusion inpainting with adaptive finite element approximations. This leads to faster inpaintings, since one replaces the fine regular pixel grid by a coarser adaptive triangulation resulting in a smaller system matrix and fewer unknowns. On the other hand, the mesh construction and corresponding sparse matrix assembly results in a non-negligible overhead. The latter two steps are also hard to parallelize, which makes it less suitable for a GPU implementation.

**Video Coding.** In the context of video compression, Peter et al. [58] proposed a method for nonlinear anisotropic diffusion inpainting. It relies on fast explicit finite difference schemes [70], which are well-suited for parallelization and benefit strongly from a good initialization available from the previous frame. With this advantage, they were able to achieve real-time decoding of  $640 \times 480$  videos on an *Nvidia GeForce GTX 460* GPU. In our work we do not utilize such temporal coherence which allows us to be more general. However, this also suggests that our methods can be made even faster when applied to videos.

Two other real-time capable video codecs that exploit temporal coherence go back to Andris et al. [2, 3]. They combine global homogeneous diffusion inpainting of keyframes with optic flow based prediction for the frames in between. In [2] they achieve real-time performance for FullHD color videos on an *Intel Xeon CPU W3565@3.20GHz*, by solving the inpainting with a multilevel conjugate gradient method [11].

**1.3. Paper Structure.** We review the basics of homogeneous diffusion inpainting in [Section 2](#). In [Section 3](#) we describe our domain decomposition approach for homogeneous diffusion inpainting. In order to accelerate the domain decomposition inpainting, specifically the convergence of the low-frequency modes of the error, we discuss how we embed it in a full multigrid framework in [Section 4](#). We evaluate our inpainting method experimentally in [Section 5](#). Finally, we conclude our paper and provide an outlook on future work in [Section 6](#).

**2. Homogeneous Diffusion Inpainting.** In this section we briefly review homogeneous diffusion inpainting [16], which is our inpainting method of choice and is used for all results in this paper. Homogeneous diffusion inpainting is a simple and very popular method for inpainting-based compression. It is parameter-free, allows to establish a comprehensive data selection theory, and may lead to particularly fast algorithms. It has been shown that, if the inpainting data is carefully chosen, we can achieve very good results [34, 37, 50, 51].

**2.1. Continuous Formulation.** Let us consider a continuous grayscale image  $f : \Omega \rightarrow \mathbb{R}$  defined on a rectangular image domain  $\Omega \subset \mathbb{R}^2$ . We store only a fraction of the full image data on a small subset  $K \subset \Omega$ . Homogeneous diffusion inpainting aims at restoring  $f$  in the inpainting domain  $\Omega \setminus K$  based only on the stored data  $f|_K$ . More specifically, the reconstruction  $u$  is obtained by using the known data  $f|_K$  as Dirichlet boundary conditions, while solving the Laplace equation on  $\Omega \setminus K$  with reflecting boundary conditions on the image

boundary  $\partial\Omega$ :

$$(2.1) \quad -\Delta u(\mathbf{x}) = 0, \quad \mathbf{x} \in \Omega \setminus K,$$

$$(2.2) \quad u(\mathbf{x}) = f(\mathbf{x}), \quad \mathbf{x} \in K,$$

$$(2.3) \quad \partial_{\mathbf{n}} u(\mathbf{x}) = 0, \quad \mathbf{x} \in \partial\Omega,$$

where  $\partial_{\mathbf{n}} u$  denotes the derivative of  $u$  in outer normal direction  $\mathbf{n}$ . For convenience, we may combine (2.1) and (2.2) into a single equation by using an indicator function  $c = \mathbb{1}_K$ , which is 1 on the known data domain  $K$  and 0 outside of it:

$$(2.4) \quad c(\mathbf{x})u(\mathbf{x}) + (1 - c(\mathbf{x}))(-\Delta)u(\mathbf{x}) = c(\mathbf{x})f(\mathbf{x}) \quad \text{on } \Omega,$$

$$(2.5) \quad \partial_{\mathbf{n}} u(\mathbf{x}) = 0 \quad \text{on } \partial\Omega.$$

**2.2. Discrete Formulation.** To apply homogeneous diffusion inpainting on a digital image  $\mathbf{f} \in \mathbb{R}^N$  with  $N$  pixels, we have to discretize (2.4) and (2.5). The discretization with finite differences leads to a linear system of equations [50, 54]. We term the approximation of the indicator function  $\mathbb{1}_K \approx \mathbf{c} \in \{0, 1\}^N$  the *inpainting mask*. Furthermore, we discretize the negated Laplacian  $-\Delta \approx \mathbf{L} \in \mathbb{R}^{N \times N}$  with reflecting boundary conditions, using the standard 5-point stencil discretization. Its values are given by

$$(2.6) \quad L_{i,j} = \begin{cases} -\frac{1}{h^2} & \text{if } j \in \mathcal{N}(i), \\ \frac{|\mathcal{N}(i)|}{h^2} & \text{if } i = j, \\ 0 & \text{else,} \end{cases}$$

where  $\mathcal{N}(i)$  are the direct (non-diagonal) neighbors of pixel  $i$ ,  $|\mathcal{N}(i)|$  is their count, and  $h$  is the distance between pixels. Then the discrete formulation of (2.4) and (2.5) is given by

$$(2.7) \quad \underbrace{(\mathbf{C} + (\mathbf{I} - \mathbf{C})\mathbf{L})}_{=: \mathbf{A}} \mathbf{u} = \underbrace{\mathbf{C}\mathbf{f}}_{=: \mathbf{b}},$$

where  $\mathbf{I} \in \mathbb{R}^{N \times N}$  is the identity matrix, and  $\mathbf{C} := \text{diag}(\mathbf{c}) \in \mathbb{R}^{N \times N}$  is a diagonal matrix with the components of the inpainting mask on the diagonal.

*Practical Considerations.* For an RGB color image, the inpainting is performed on each of the three channels separately. Thus, we get three linear systems of this type with different right-hand sides. While  $\mathbf{A}\mathbf{u} = \mathbf{b}$  is not symmetric, it can be reduced to a symmetric and positive-definite system by removing the mask pixels [50]. Since the extended system (2.7) acts exactly the same as the reduced one at all unknown pixels, we can solve it with a conjugate gradient method (CG) [32]. For highly parallel hardware such as GPUs, solving the global homogeneous diffusion inpainting system with a CG method is, however, not very efficient compared to domain decomposition methods. The reason for this lies on the one hand in the global scalar products which entail two global synchronizations in each iteration, but on the other hand also in the extensive use of global GPU memory, which is quite slow. Domain decomposition methods, instead, require only a single global scalar product per iteration and can use faster local GPU memory for the local problems on the subdomains. This makes them much more efficient on highly parallel GPUs. For these reasons we discuss domain decomposition methods in the following section and specifically our method of choice: the optimized restricted additive Schwarz method (ORAS) [65].

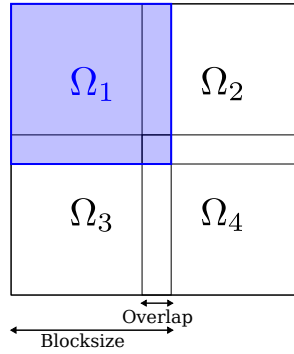


Figure 1: **Domain Decomposition Example.** The domain is divided into four overlapping subdomains. The subdomain  $\Omega_1$  is highlighted in blue.

**3. Optimized Restricted Additive Schwarz.** The *restricted additive Schwarz (RAS)* method [15], in its continuous formulation, is an iterative technique for solving boundary value problems, such as (2.1)–(2.3). It is one of the simplest domain decomposition methods [22, 68] and is well suited for parallelization. As a first step, the image domain  $\Omega$  is divided into  $k \in \mathbb{N}$  overlapping subdomains  $\Omega_1, \dots, \Omega_k \subset \Omega$ , such that  $\cup_{i=1}^k \Omega_i = \Omega$ . An example of such an overlapping division into four subdomains is shown in Figure 1. In the continuous setting,

---

**Algorithm 3.1** RAS for Homogeneous Diffusion Inpainting: Continuous Formulation

---

1. Compute the global residual  $r^n : \Omega \rightarrow \mathbb{R}$ :

$$(3.1) \quad r^n(\mathbf{x}) = \begin{cases} 0 + \Delta u^n(\mathbf{x}) & \text{for } \mathbf{x} \in \Omega \setminus K, \\ 0 & \text{for } \mathbf{x} \in K. \end{cases}$$

2. For  $i \in \{1, \dots, k\}$  solve the following PDE for the local correction  $v_i^n$ :

$$(3.2) \quad -\Delta v_i^n(\mathbf{x}) = r^n(\mathbf{x}) \quad \mathbf{x} \in \Omega_i \setminus K,$$

$$(3.3) \quad v_i^n(\mathbf{x}) = r^n(\mathbf{x}) \quad \mathbf{x} \in \Omega_i \cap K,$$

$$(3.4) \quad \partial_{\mathbf{n}} v_i^n(\mathbf{x}) = 0 \quad \mathbf{x} \in \partial\Omega_i \cap \partial\Omega,$$

$$(3.5) \quad v_i^n(\mathbf{x}) = 0 \quad \mathbf{x} \in \partial\Omega_i \setminus \partial\Omega.$$

3. Update  $u^n$  with the extensions of the weighted local corrections  $v_i^n$ :

$$(3.6) \quad u^{n+1}(\mathbf{x}) = u^n(\mathbf{x}) + \sum_{i=1}^k E_i(\chi_i(\mathbf{x})v_i^n(\mathbf{x})).$$


---

the RAS method is given by iterating Algorithm 3.1. Starting with an initial approximation  $u^0 : \Omega \rightarrow \mathbb{R}$  that fulfills the interpolation condition  $u^0|_K = f|_K$  at the known locations, in each iteration  $n$ , we try to correct the current approximation  $u^n$  by locally computing

correction terms  $v_i : \Omega_i \rightarrow \mathbb{R}$  to the global error  $e^n = u - u^n$  for every subdomain. We obtain these local corrections by solving local versions of the global PDE, but with the global residual  $r^n$  as the right-hand side. At the subdomain boundaries which are not part of the global image boundary, the so-called inner subdomain boundaries, we need additional boundary conditions. There we impose homogeneous Dirichlet conditions. Together with the homogeneous Neumann conditions at the image boundaries and the Dirichlet conditions at the mask points, we get local PDEs with conditions over three different sets:  $\partial\Omega_i \cap \partial\Omega$ ,  $\partial\Omega_i \setminus \partial\Omega$ , and  $\Omega_i \cap K$ . We extend the local corrections  $v_i$  from functions on  $\Omega_i$  to functions on  $\Omega$ , with an extension operator  $E_i(v_i) : \Omega \rightarrow \mathbb{R}$  that sets them to zero outside of  $\Omega_i$ . This allows us to add them to the global solution  $u^n$ . However, if we simply add the corrections from all subdomains to the global solution, we would add multiple corrections in the overlapping regions. This would result in divergence; see e.g. [24, 27]. In order to achieve convergence, we have to weight the local corrections in the overlapping regions before adding them to the global solution, by defining partition of unity functions  $\chi_i : \Omega_i \rightarrow \mathbb{R}$ , such that

$$(3.7) \quad w = \sum_{i=1}^k E_i(\chi_i w|_{\Omega_i})$$

holds for any function  $w : \Omega \rightarrow \mathbb{R}$ . This ensures that at every point the weights always add up to 1. As we iterate this method,  $u^n$  converges towards the solution  $u$  of the global PDE, as long as the subdomains overlap. The convergence speed of RAS depends on the size of the overlap as well as the overall number of subdomains.

By replacing the inner subdomain boundary conditions with mixed Robin boundary conditions, we can optimize the communication between neighboring subdomains. This improves the convergence speed of the method. The resulting algorithm is then called the *optimized restricted additive Schwarz (ORAS)* method [65]. This means that we replace the Dirichlet boundary conditions (3.5) with mixed boundary conditions,

$$(3.8) \quad \partial_{\mathbf{n}} v_i^n(\mathbf{x}) + \alpha \cdot v_i^n(\mathbf{x}) = 0 \quad \mathbf{x} \in \partial\Omega_i \setminus \partial\Omega,$$

where  $\alpha > 0$  is a weighting factor between the Dirichlet and the Neumann condition.

**Discrete Optimized Restricted Additive Schwarz.** In the discrete case we have to solve a sparse linear system of equations (2.7). To this end, the discrete image domain  $\Omega$  with  $N$  pixels is also divided into  $k$  overlapping domains  $\Omega_1, \dots, \Omega_k \subset \Omega$  such that  $\cup_{i=1}^k \Omega_i = \Omega$ . We define restriction matrices  $\mathbf{R}_i \in \mathbb{R}^{|\Omega_i| \times N}$ , where  $|\Omega_i|$  is the number of pixels in subdomain  $\Omega_i$ , that restrict global vectors to the local domains by extracting the values from the subdomain  $\Omega_i$  and ignoring all values outside of it. Their transposes  $\mathbf{R}_i^\top$  are then extension matrices analogues to  $E_i$  from the continuous case, that extend local vectors from the subdomain  $\Omega_i$  to the global domain  $\Omega$ .

For the discrete counterpart of the partition of unity functions  $\chi_i$ , we define diagonal nonnegative matrices  $\mathbf{D}_i \in \mathbb{R}^{|\Omega_i| \times |\Omega_i|}$ , such that

$$(3.9) \quad \mathbf{I} = \sum_{i=1}^k \mathbf{R}_i^\top \mathbf{D}_i \mathbf{R}_i,$$

where  $\mathbf{I} \in \mathbb{R}^{N \times N}$  is the identity matrix of size  $N \times N$ . The latter implies the discrete counterpart  $\mathbf{w} = \sum_{i=1}^k \mathbf{R}_i^\top \mathbf{D}_i \mathbf{R}_i \mathbf{w}$  of the condition (3.7).

The local corrections  $\mathbf{v}_i^n$  are computed by solving small linear systems, where the system matrices  $\mathbf{A}_i$  are given by restricting the global system matrix  $\mathbf{A}$  to the subdomains  $\Omega_i$  and imposing mixed Robin boundary conditions at the inner subdomain boundaries. Starting with an initial guess  $\mathbf{u}^0$  the resulting discrete ORAS method is given by iterating Algorithm 3.2.

---

**Algorithm 3.2** ORAS for Homogeneous Diffusion Inpainting: Discrete Formulation

---

1. Compute the global residual  $\mathbf{r}^n \in \mathbb{R}^N$ :

$$(3.10) \quad \mathbf{r}^n = \mathbf{b} - \mathbf{A}\mathbf{u}^n$$

2. For  $i \in \{1, \dots, k\}$  solve for a local correction  $\mathbf{v}_i^n$ :

$$(3.11) \quad \mathbf{A}_i \mathbf{v}_i^n = \mathbf{R}_i \mathbf{r}^n$$

3. Update  $\mathbf{u}^n$  with the weighted and extended local corrections  $\mathbf{v}_i^n$ :

$$(3.12) \quad \mathbf{u}^{n+1} = \mathbf{u}^n + \sum_{i=1}^k \mathbf{R}_i^\top \mathbf{D}_i \mathbf{v}_i^n$$


---

**3.1. Implementation Details.** Even though domain decomposition methods are typically used as preconditioners for Krylov methods such as CG, in the current work we use them directly. Due to the approximately local influence of each mask pixel, the global coupling from Krylov methods is not necessary for us. As global Krylov methods need several synchronizations per iteration and rely on global GPU memory, using ORAS as a direct method is more efficient for our GPU implementation. In our ORAS inpainting method we decompose the image domain into multiple overlapping blocks of size  $32 \times 32$  pixels with an overlap of 6 pixels. These values are optimized for our *Nvidia GeForce GTX 1080 Ti* GPU, which results in 36852 local problems in each iteration of the ORAS method for a 4K color image. The local problems are solved using a simple conjugate gradient algorithm [60]. We stop the local CG iterations on a block when the squared 2-norm of the residual has been reduced to a fixed fraction of the squared global residual norm. Compared to a stopping criterion based on the local relative residual norm, this leads to a more uniform convergence, since all blocks have the same squared residual norm after each ORAS iteration. This also avoids using unnecessarily many CG iterations in blocks that are already sufficiently converged. For the weight matrices  $\mathbf{D}_i$ , we use separable weights in  $x$ - and  $y$ -direction, which means we only have to ensure that the partition of unity holds for an overlap between two blocks in a single direction. Figure 2 visualizes our weighting. For the outermost pixels we have to use a weight of 0 to ensure convergence [65], which leads to a weight of 1 for the innermost pixel in the overlapping region. In between, we use a linear weighting, such that both weights add up to 1.

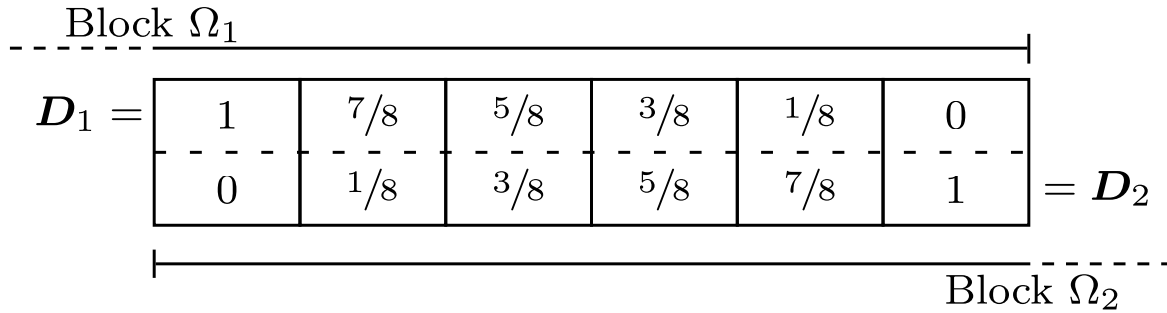


Figure 2: **Visualization of the Overlap Weights.** The weights  $D_1$  and  $D_2$  in the overlap of two blocks  $\Omega_1$  and  $\Omega_2$  are chosen, such that they always add up to 1 at each pixel.

**4. Embedding ORAS in Multigrid.** Simple domain decomposition methods such as ORAS have one drawback: They only allow communication between neighboring blocks, so it takes many iterations to spread information over large distances. Thus, high frequencies of the error are reduced much faster than low frequencies. This leads to a fast convergence rate at the beginning, which slows down significantly after the first few iterations. As a remedy, domain decomposition methods are usually used together with a simple two-level scheme [22, 68]. Besides the local subdomain corrections, it computes an additional correction on a very coarse grid to couple all subdomains together. This helps to better attenuate the low-frequency error components. As the influence area of each mask pixel in homogeneous diffusion inpainting is approximately localized, such a global coupling of all subdomains is not really necessary. Instead, a more fine-grained coupling between subdomains is more useful.

Multigrid methods [12, 14, 31, 69, 71] can offer such a coupling between subdomains. They compute useful correction steps on coarser levels to improve the convergence of the low-frequency error components. In the next section we describe a simple two level multigrid method.

**4.1. Two-Grid Cycle.** Iterative solvers such as Jacobi [60], Gauss-Seidel [60], or the ORAS method [65] reduce the high frequency modes of the error efficiently, but they are much slower at decreasing the low frequencies. Multigrid addresses this by transferring the problem to a coarser grid where the low frequencies appear as higher frequencies which can be reduced more efficiently by the very same solvers. We first study the two grid formulation of multigrid which consist of iterating what's known as a *two-grid cycle*. Our two grids are the original fine grid with grid spacing  $h$ , and a coarser grid with spacing  $H > h$ . In our implementation, we set  $H = 2h$ .

We start the cycle  $k + 1$  with an approximation  $\mathbf{u}_h^k$  of the solution  $\mathbf{u}_h$  of the problem  $\mathbf{A}_h \mathbf{u}_h = \mathbf{b}_h$ . Here  $\mathbf{A}_h$  is the original system matrix and  $\mathbf{b}_h$  is the right-hand side (both on the original fine grid). If we knew the true error  $\mathbf{u}_h - \mathbf{u}_h^k$  we could correct our approximation to get the true solution:  $\mathbf{u}_h^k + (\mathbf{u}_h - \mathbf{u}_h^k) = \mathbf{u}_h$ . Consequently, our goal is to find an approximation of the error efficiently, by using the aforementioned idea of decimating different frequencies of the error over different grids. The error  $\mathbf{u}_h - \mathbf{u}_h^k$  typically contains both high- and low-frequency components. We reduce the high frequencies by performing a few iterations  $\vartheta_{\text{pre}}$

with a *smoother*: an iterative solver that dampens the high frequencies efficiently - e.g. damped Jacobi, Gauss-Seidel, or in our case ORAS. This results in the approximation of the solution

$$(4.1) \quad \mathbf{u}_h^{k+1/3} = \text{pre-smooth}(\mathbf{A}_h, \mathbf{b}_h, \mathbf{u}_h^k, \vartheta_{\text{pre}}).$$

Provided we have used enough iterations  $\vartheta_{\text{pre}}$ , the error  $\mathbf{e}_h^k = \mathbf{b}_h - \mathbf{u}_h^{k+1/3}$  will have only negligible high-frequency components. We can then represent it almost perfectly on the coarser grid. The transfer between the grids can be formalized using a restriction matrix  $\mathbf{R}_h^H$  and a prolongation matrix  $\mathbf{P}_H^h$ . The two are designed so that sufficiently low frequency components are reproduced exactly, while higher frequency components are smoothed out to avoid aliasing.

A problem of the above formulation is that we do not know the error in practice, so we cannot transfer it to the coarser grid. However, we know the residual and its relation to the error:

$$(4.2) \quad \mathbf{r}_h^k = \mathbf{b}_h - \mathbf{A}_h \mathbf{u}_h^{k+1/3} = \mathbf{A}_h \mathbf{u}_h - \mathbf{A}_h \mathbf{u}_h^{k+1/3} = \mathbf{A}_h (\mathbf{u}_h - \mathbf{u}_h^{k+1/3}) = \mathbf{A}_h \mathbf{e}_h^k.$$

On the coarse grid this reads  $\mathbf{A}_H \mathbf{e}_H^k = \mathbf{r}_H^k$ , where  $\mathbf{A}_H$  is an analogue of  $\mathbf{A}_h$  on the lower level. To compute  $\mathbf{A}_H$ , we discretize the inpainting problem on the coarser grid (see [Subsection 4.3](#)). We get the coarse residual  $\mathbf{r}_H^k$  by transferring the fine grid residual  $\mathbf{r}_h^k$  to the coarse grid:

$$(4.3) \quad \mathbf{r}_H^k = \mathbf{R}_h^H \mathbf{r}_h^k.$$

In the two-grid cycle we then solve the coarse grid problem for the error exactly:

$$(4.4) \quad \mathbf{A}_H \mathbf{e}_H^k = \mathbf{r}_H^k.$$

We note that the matrix  $\mathbf{A}_H$  is twice smaller in each dimension compared to  $\mathbf{A}_h$ , thus the computational cost is also reduced. We can then transfer  $\mathbf{e}_H^k$  to the fine grid by using the prolongation matrix  $\tilde{\mathbf{e}}_h^k = \mathbf{P}_H^h \mathbf{e}_H^k$  and use it to correct our approximation of the solution:

$$(4.5) \quad \mathbf{u}_h^{k+2/3} = \mathbf{u}_h^{k+1/3} + \tilde{\mathbf{e}}_h^k = \mathbf{u}_h^{k+1/3} + \mathbf{P}_H^h \mathbf{e}_H^k.$$

A subsequent post-smoothing with  $\vartheta_{\text{post}}$  iterations is then applied to smooth high frequency error components potentially introduced by the correction step:

$$(4.6) \quad \mathbf{u}_h^{k+1} = \text{post-smooth}(\mathbf{A}_h, \mathbf{b}_h, \mathbf{u}_h^{k+2/3}, \vartheta_{\text{post}}).$$

All of these steps together result in [Algorithm 4.1](#). While solving  $\mathbf{A}_H \mathbf{x}_H = \mathbf{b}_H$  is generally computationally cheaper than solving  $\mathbf{A}_h \mathbf{x}_h = \mathbf{b}_h$ , for high resolution images even the coarse problem is expensive. Thus, one often considers recursively applying this process over a sequence of grids with decreasing resolution until a grid of a sufficiently low resolution is reached. The latter results in an almost optimal workload of  $O(N \log N)$  for computing the solution. Another issue is how to choose a good initial guess  $\mathbf{u}_h^0$ . It turns out that a good quality guess can be constructed efficiently by starting from the coarsest level. The recursive approach with this initial guess has an optimal workload of  $O(N)$ . Both of these ideas are discussed in the following subsection.

**Algorithm 4.1** Two-Grid Cycle

1. Pre-smooth:  $\mathbf{u}_h^{k+1/3} = \text{ORAS}(\mathbf{A}_h, \mathbf{b}_h, \mathbf{u}_h^k, \vartheta_{\text{pre}})$
2. Compute Residual:  $\mathbf{r}_h^k = \mathbf{b}_h - \mathbf{A}_h \mathbf{u}_h^{k+1/3}$
3. Restriction:  $\mathbf{r}_H^k = \mathbf{R}_H^h \mathbf{r}_h^k$
4. Coarse Solve:  $\mathbf{A}_H \mathbf{e}_H^k = \mathbf{r}_H^k$
5. Prolongation + Correction:  $\mathbf{u}_h^{k+2/3} = \mathbf{u}_h^{k+1/3} + \mathbf{P}_H^h \mathbf{e}_H^k$
6. Post-smooth:  $\mathbf{u}_h^{k+1} = \text{ORAS}(\mathbf{A}_h, \mathbf{b}_h, \mathbf{u}_h^{k+2/3}, \vartheta_{\text{post}})$

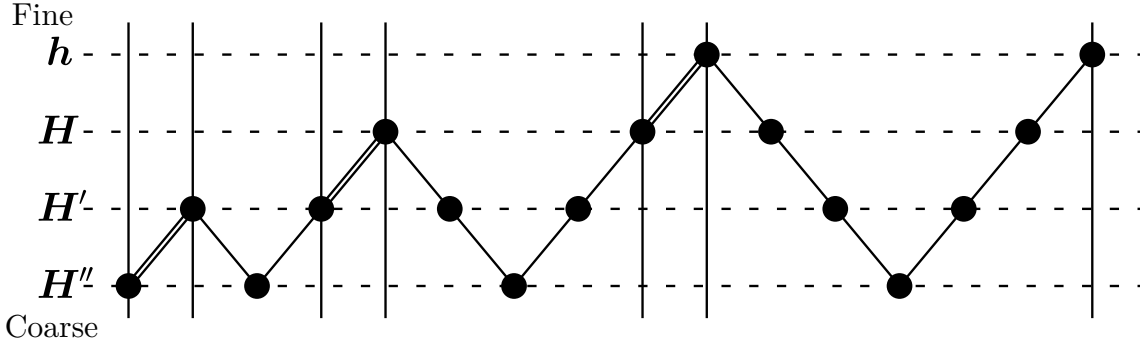


Figure 3: **Full Multigrid Scheme.** Example with four resolution layers and a single V-cycle for each level. The doubled lines represent the FMG prolongations to initialize the V-cycle for the next finer level.

**4.2. V-Cycles and Full Multigrid.** Instead of using only two resolution levels, we can extend the two-grid cycle to multiple levels, which allows to efficiently dampen different frequencies of the error at different resolutions. The solve on the coarse level can be replaced by another correction step on an even coarser level. This process can be iterated recursively until we reach a level that is coarse enough for the lowest possible frequencies in our problem. The hierarchical application of the two-grid cycle is called a *V-cycle*.

Moreover, we can speed up the computation even further by providing a good initialization. Such an initialization can be obtained by computing an inpainting solution on a coarser grid and prolongating it to the fine resolution. This can be extended to a complete coarse-to-fine initialization strategy. Starting from a very coarse resolution grid, we successively refine the problem, where inpainting solutions from coarser levels are interpolated and used as an initialization for finer ones. At each level a V-cycle is used to solve the resulting linear system. This coarse-to-fine method with the error correction steps is called *full multigrid (FMG)*. Figure 3 shows an illustration how the different grids are traversed in such an FMG scheme. However, restriction and prolongation between different grids can be costly in terms of runtime on parallel hardware such as GPUs, as they consist mainly of global memory operations. To reduce the amount of restriction and prolongation operations without losing the advantages of FMG, we propose to skip the V-cycles on the lower levels and just use a single pre-smoothing iteration instead. This reduced FMG scheme, is depicted in Figure 4. For homogeneous dif-

fusion inpainting, this reduced FMG scheme is sufficient for a good convergence and improves the overall runtime compared to the non-reduced scheme.

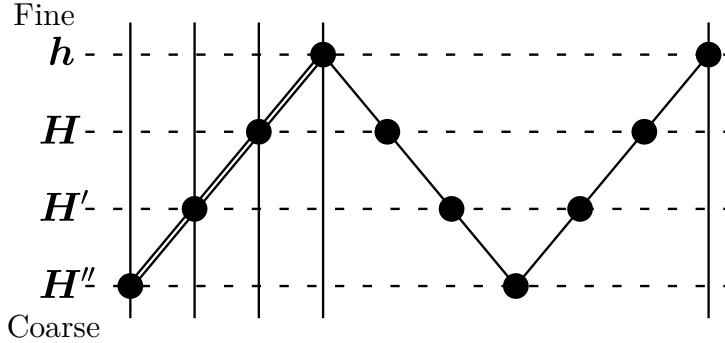


Figure 4: **Reduced Full Multigrid Scheme.** The initial guess is constructed in a coarse-to-fine manner, also known as one-way or cascadic multigrid. Then we continue with additional V-cycle correction steps (a single V-cycle is visualized above).

**4.3. Lower Resolution Problems Construction.** Full multigrid requires constructing a problem  $\mathbf{A}_H \mathbf{u}_H = \mathbf{b}_H$  on the coarser grid that is similar enough to the problem  $\mathbf{A}_h \mathbf{u}_h = \mathbf{b}_h$  on the finer grid. To achieve this, we use a downsampling ratio of two in each direction so that the difference between the two problems is as small as possible. We note that in the multigrid literature the standard considered boundary is rectangular, and thus its connectivity and geometry remains the same under downsampling. In our case, only the reflecting Neumann boundary is on the rectangle corresponding to the image boundary. The Dirichlet boundary given by the mask  $\mathbf{c}$  can be arbitrarily complex and usually consists of scattered pixels with largely varying density over the image domain. This means that both the geometry and connectivity of our Dirichlet boundary greatly changes with downsampling. This is important, as it is known that grid transfer operations in multigrid have to be adapted near the boundary for optimal performance [71].

*Mask Downsampling.* In order to construct coarser versions of the mask  $\mathbf{c}$ , we use a specific dyadic downsampling: A pixel on the coarser level becomes a mask pixel if any one of its corresponding pixels on the finer level is a mask pixel (max pooling as opposed to average pooling). For an illustration of this process, see Figure 5. This is similar in spirit to what is done in [53], but there the authors deal with simpler boundaries. We note that the density of the boundary set increases as we downsample in this manner, which generally makes solutions on the coarser grid more efficient. At the same time, however, on coarser levels the boundary’s geometry and even connectivity changes, such that our coarsest problem discretization is quite far removed from the initial fine grid problem. This explains for instance why a multigrid preconditioned conjugate gradient solver is not a good fit for our problem, or why downsampling with an aggressive ratio, as done in standard multilevel domain decomposition methods, is not optimal for our problem.

*Naïve Mask Values Downsampling.* Besides for the mask, we also need to find lower resolution counterparts  $\mathbf{b}_H = \mathbf{C}_H \mathbf{f}_H$  for the mask values  $\mathbf{b}_h = \mathbf{C}_h \mathbf{f}_h$ . The naïve downsampling

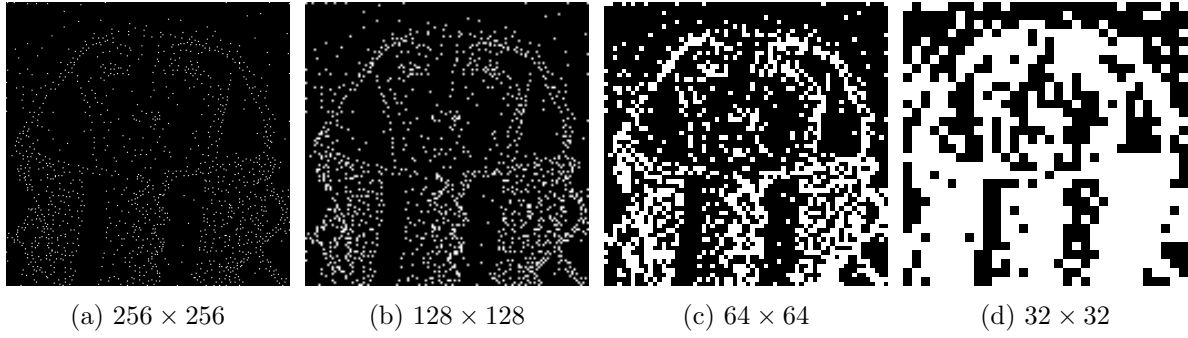


Figure 5: **Mask Restriction Example on *trui* with a 2% Mask Density.** With each resolution level the mask density increases while the connectivity of the mask changes.

averages the values of all mask pixels in a  $2 \times 2$  neighborhood on the finer level. If there are no mask pixels in the neighborhood, the corresponding coarse level pixel itself is not considered as a mask pixel and thus the right-hand side should be set to 0. As an example, the naïve coarse level right-hand side  $b_H^{2,2}$  for the coarse level pixel  $c_H^{2,2}$  is given by

$$(4.7) \quad \begin{array}{|c|c|} \hline c_h^{3,3} & c_h^{4,3} \\ \hline c_h^{3,4} & c_h^{4,4} \\ \hline \end{array}, \quad \begin{array}{|c|c|} \hline b_h^{3,3} & b_h^{4,3} \\ \hline b_h^{3,4} & b_h^{4,4} \\ \hline \end{array}, \quad b_H^{2,2} = \frac{c_h^{3,3}b_h^{3,3} + c_h^{3,4}b_h^{3,4} + c_h^{4,3}b_h^{4,3} + c_h^{4,4}b_h^{4,4}}{\max\left(1, c_h^{3,3} + c_h^{4,3} + c_h^{3,4} + c_h^{4,4}\right)}.$$

As one may expect with such a complex boundary, it turns out that the above simple averaging and downscaling is not ideal. A naïve average mixes as many as four mask values from the finer level to get the value of the corresponding mask pixel on the coarser level. However, a key observation specific to homogeneous diffusion inpainting is that the influence of a mask pixel is localized to regions enclosed by other mask pixels. This means that a naïve downsampling can cause mask pixels, that had a localized effect on the finer level, to have their influence leak over boundaries on the coarser level: note the pronounced color bleeding near edges in [Figure 6\(a\)](#). To rectify this, we modify the downsampling procedure for the mask values by allowing mask pixels to suppress the contribution of their neighbors.

**Modified Mask Values Downsampling.** If the four neighbors of a mask pixel are also mask pixels, then its value should not be averaged on the lower level, since its influence is suppressed by its neighbors. Note that the neighbors can be either fine scale or coarse scale mask pixels, since either will suppress the influence of the pixel provided that they are its direct neighbors. As an example we consider the fine mask pixel  $c_h^{3,3}$ , then its direct neighbors are: its fine grid neighbors  $c_h^{3,4}$  and  $c_h^{4,3}$ , and its coarse grid neighbors  $c_H^{1,2}$  and  $c_H^{2,1}$ . An illustration of this is presented below, where the coarse pixel  $c_H^{2,2}$  is split into its fine scale constituents  $c_h^{3,3}$ ,  $c_h^{3,4}$ ,  $c_h^{4,3}$ ,  $c_h^{4,4}$ .



(a) naïve downsampling

(b) modified downsampling

Figure 6: **Downsampling Leakage Example.** Illustration of the leakage caused by naïve dyadic downsampling for a 2% mask using only one-way multigrid.

$$(4.8) \quad \begin{array}{|c|c|c|} \hline * & c_H^{2,1} & * \\ \hline c_H^{1,2} & \begin{array}{|c|c|} \hline c_h^{3,3} & c_h^{4,3} \\ \hline c_h^{3,4} & c_h^{4,4} \\ \hline \end{array} & c_H^{3,2} \\ \hline * & c_H^{2,3} & * \\ \hline \end{array}$$

To model this suppression effect, we may assign each fine grid pixel a weight in the averaging based on the number of its non-mask pixel neighbors. This yields the following modified downsampling procedure for  $b_H^{2,2}$ :

$$(4.9) \quad \begin{aligned} w_h^{3,3} &= c_h^{3,3} \left( 4 - c_H^{1,2} - c_H^{2,1} - c_h^{4,3} - c_h^{3,4} \right), & w_h^{3,4} &= c_h^{3,4} \left( 4 - c_H^{1,2} - c_h^{3,3} - c_h^{4,3} - c_H^{2,3} \right), \\ w_h^{4,3} &= c_h^{4,3} \left( 4 - c_h^{3,3} - c_H^{2,1} - c_H^{3,2} - c_h^{3,4} \right), & w_h^{4,4} &= c_h^{4,4} \left( 4 - c_h^{3,3} - c_h^{3,3} - c_H^{3,2} - c_H^{2,3} \right), \end{aligned}$$

$$(4.10) \quad b_H^{2,2} = \frac{w_h^{3,3} b_h^{3,3} + w_h^{3,4} b_h^{3,4} + w_h^{4,3} b_h^{4,3} + w_h^{4,4} b_h^{4,4}}{\max \left( 1, w_h^{3,3} + w_h^{3,4} + w_h^{4,3} + w_h^{4,4} \right)}.$$

The effect of this modification is illustrated in [Figure 6\(b\)](#), which exhibits much less color bleeding than [Figure 6\(a\)](#). While the latter could be rectified with more V-cycles or complex smoothers, the modified downsampling allows to diminish such artifacts at a very low computational cost.

**4.4. Implementation Details.** For our multigrid ORAS inpainting method, we use a single V-cycle on the finest level, and we set the pre- and post-smoothing iterations to a single ORAS iteration. We choose the number of levels such that the coarsest level consists of a single ORAS

block of size  $32 \times 32$  pixels. Since we reduce the resolution by two in each direction with each level, we get a total of 8 resolution levels for a 4K image.

For the restriction outside of the mask pixels we employ a simple averaging. The prolongation to a finer grid is implemented with bilinear interpolation, except at the mask pixels from the fine grid where we have to fulfill the interpolation conditions. The prolonged coarse grid solutions, used in the initial cascadic part, are set to the corresponding values from the right-hand side at the mask pixels such that the interpolation condition  $C_h P_H^h u_H = C_h f_h$  is satisfied. We set the prolonged coarse grid corrections to zero at the mask pixels, since the residual is always zero there.

**5. Experiments.** After mentioning the technical details of our experimental setup in [Subsection 5.1](#), we show the improvements of our full multigrid ORAS inpainting in comparison to our previous ORAS multilevel inpainting [42] in [Subsection 5.2](#).

**5.1. Experimental Setup.** For the experimental evaluation of our full multigrid ORAS inpainting, we compare against the multilevel ORAS approach from our conference contribution [42] and CG, as these methods are suitable for parallelization and can be efficiently implemented on a GPU. To allow for a fair comparison, we also implement multilevel and multigrid variants of CG that use the same framework as their ORAS-based counterparts, but with CG as a pre- and post-smoothing operator. We excluded other inpainting solvers such as the Green’s functions inpainting [4, 35] from our comparisons, since they become infeasible for large images due to runtime and memory restrictions.

We conducted our experiments on an *AMD Ryzen 5900X@3.7GHz* and an *Nvidia GeForce GTX 1080 Ti* GPU. We used state-of-the-art optimized inpainting masks, obtained with a Delaunay densification strategy, proposed in the second part of this companion paper [41]. To enable a representative evaluation of our inpainting method, we performed our experiments on twelve 4K photographs that contain a varying amount of texture and coarse and fine structures (see [Figures 7](#) and [8](#)). [Figures 7](#) and [8](#) also show the optimized inpainting masks for a density of 5% and the corresponding inpainting results obtained with our multigrid ORAS solver. We achieve an average runtime of 14.3 milliseconds, which corresponds to **a frame rate of nearly 70 frames per second**.

**5.2. Inpainting Experiments.** In [Figure 9](#) we compare our multilevel and multigrid ORAS inpainting algorithms with their corresponding CG counterparts on different densities from 0.5% to 10%, averaged over all twelve 4K images.

*Stopping Criterion.* As a stopping criterion we use the relative decay of the Euclidean norm of the residual. We note that this alone is not a good indicator of the true reconstruction error, which can be seen in [Figure 9\(a\)](#). It shows the approximation quality with respect to a fully converged inpainting result for a relative residual norm of  $10^{-3}$ . For multilevel and multigrid methods, we obtain reasonably good approximation qualities for all mask densities. Our ORAS multigrid method even outperforms all other methods. The results for both single level methods are, however, clearly not fully converged and would require a much stricter stopping criterion for a reasonable approximation quality. Due to this, we only consider multilevel and multigrid methods from this point on, as they are clearly superior. We use a relative residual norm of  $10^{-3}$  as a stopping criterion, as we have seen that this is sufficient

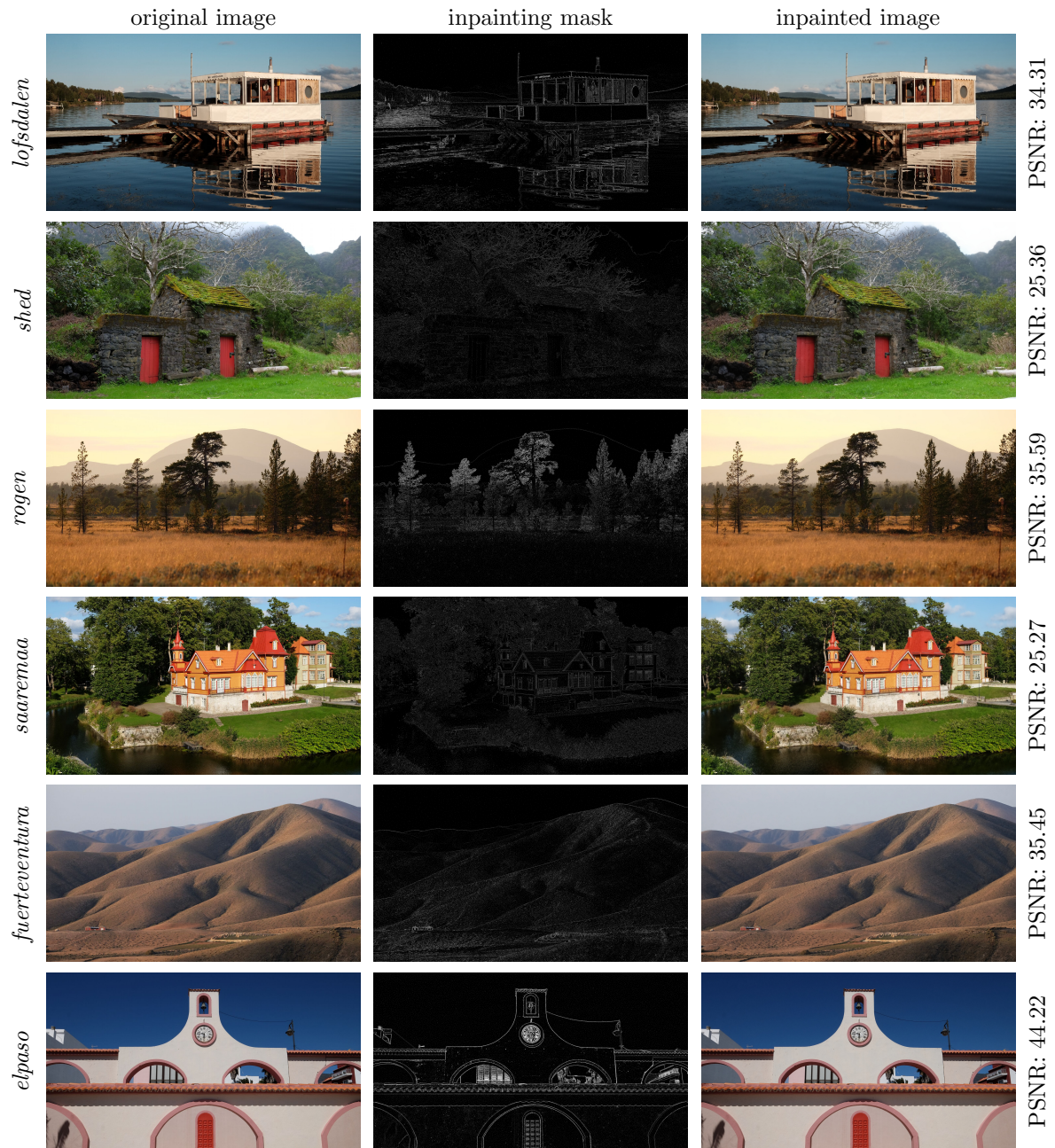


Figure 7: **Sparse Inpainting with 5 % Known Data.** Images 1 to 6 of our test dataset of size  $3840 \times 2160$  with an 5% optimized inpainting mask and the corresponding inpainting. Photos by J. Weickert.

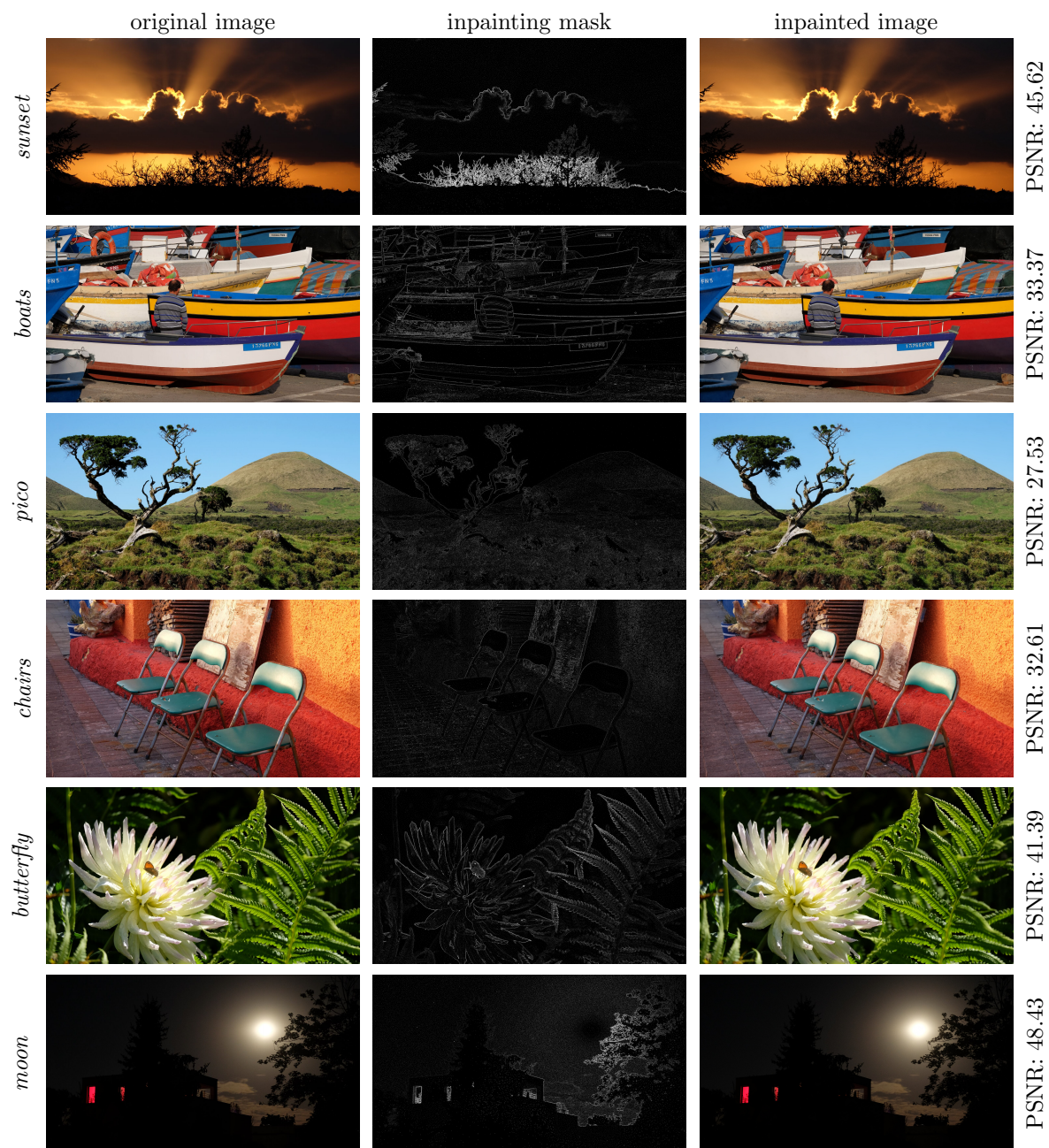


Figure 8: **Sparse Inpainting with 5 % Known Data.** Images 7 to 12 of our test dataset of size  $3840 \times 2160$  with an 5% optimized inpainting mask and the corresponding inpainting. Photos by J. Weickert.

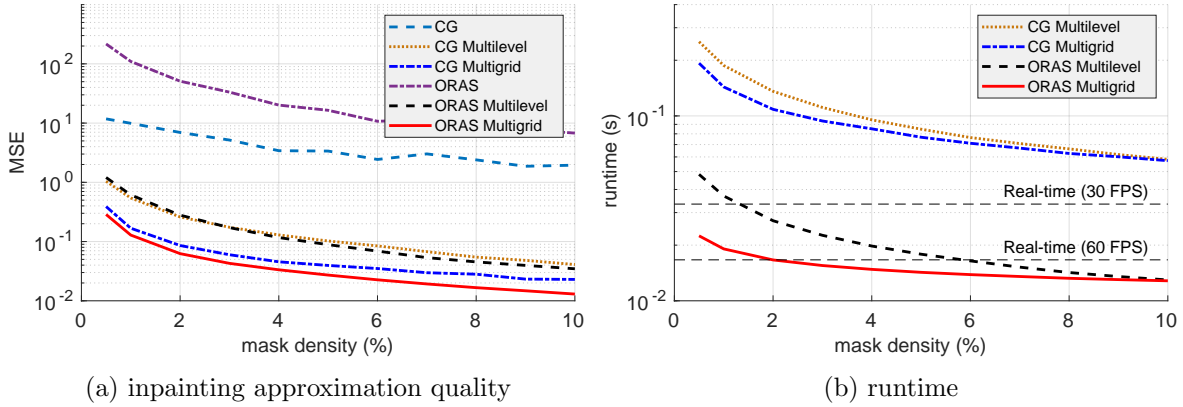


Figure 9: **Inpainting Comparison for Different Mask Densities.** (a) MSE between the inpainting approximation and a converged inpainting for a stopping criterion of  $10^{-3}$ . The multigrid methods are closest to the converged inpainting with our ORAS multigrid performing the best. Both single-level methods are clearly not fully converged and would require a much stricter stopping criterion for a reasonable approximation quality. (b) Runtimes of multilevel and multigrid methods for a stopping criterion of  $10^{-3}$ . Our ORAS-based methods are more than 4 times faster than their corresponding CG counterparts. Only the ORAS multigrid methods achieve real-time performance for all densities.

for the multilevel and multigrid methods.

**Mask Density Runtime Scaling.** Figure 9(b) shows the corresponding inpainting runtimes. We observe that the domain decomposition methods clearly outperform their corresponding CG-based solvers by more than a factor of 4. This demonstrates the capabilities of domain decomposition methods over simpler algorithms. While the performance of the ORAS multigrid and the ORAS multilevel method is similar for a mask density of 10%, our multigrid method clearly outperforms the multilevel approach for lower mask densities. This is because even though both methods use a coarse-to-fine initial guess, only multigrid performs V-cycles that efficiently reduce lower frequency error modes. Since for sparser masks the mask pixel contributions are lower frequency, those masks benefit much more from the multigrid approach. This allows us to perform real-time inpainting with 30 frames per second for all tested densities and even 60 frames per second for mask densities higher than 2%.

**Resolution Runtime Scaling.** To evaluate our inpainting methods over different image sizes, we conduct experiments over resolutions ranging from  $480 \times 270$  to  $3840 \times 2160$  with 5% masks. The results are shown in Figure 10. We can see that similar to the results from Figure 9(b), our ORAS-based inpainting methods are over four times faster than their CG-based counterparts on all image resolutions. While both of our domain decomposition methods are able to inpaint 4K images in real-time, with at least 30 frames per second, the CG-based methods achieve this only for FullHD resolutions. Figure 10 also reveals that, at least for higher image resolutions, all four methods show a nearly linear behavior in the double logarithmic plot. As the slope is

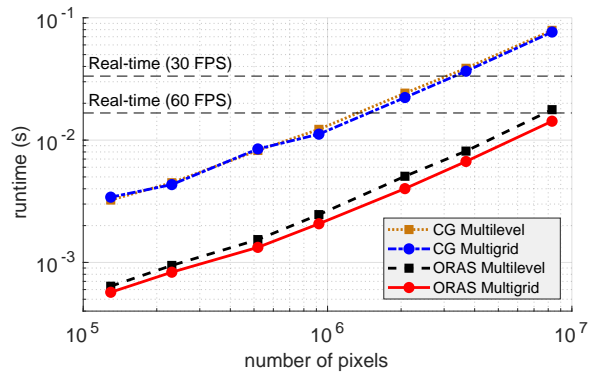


Figure 10: **Comparison on Different Resolution Levels for a 5% Mask Density.** The horizontal dashed lines represent real-time inpainting with 30 and 60 frames per second. Our ORAS multigrid method achieves more than 60 frames per second for a 4K resolution (last data point). With CG-based methods we achieve real-time performance only up to a FullHD resolution (third data point from the right) and only with approximately 45 frames per second.

approximately 1 for all methods, we observe an ideal linear scaling behavior.

**6. Conclusions and Outlook.** One of the biggest challenges in inpainting-based compression has been the high computational complexity associated with inpainting algorithms. While qualitatively those are a viable alternative to transform-based approaches, standard solvers result in long inpainting runtimes for larger images. Our work substantially alleviates this issue. By adapting and fusing two of the most efficient concepts of numerical analysis and taking advantage of the computing power of modern parallel hardware, we have obtained a very efficient solver for homogeneous diffusion inpainting. This enabled us, for the first time ever, to achieve homogeneous diffusion inpainting at 60 frames per second for 4K color images on a contemporary GPU (in actuality four generations old). This suggests that even 8K resolution in real-time would be possible with the latest generation of GPUs. Furthermore, most state-of-the-art methods for data optimization on the encoding side rely on multiple inpaintings. Thus, our work not only benefits the decoding side but is also able to improve the runtime of encoding methods. This demonstrates that inpainting-based compression has left its infancy to become a serious alternative to classical transform-based codecs not only in terms of quality but also for real-time applications.

Our experience with homogeneous diffusion inpainting suggests that approaches like ours, which judiciously adapt multiple numerical methods and exploit modern parallel architectures, could also be successfully transferred to numerous other image processing tasks.

Last but not least, while our work mainly focuses on mathematically sound algorithms, we have nevertheless extracted interesting insights about the structure of homogeneous diffusion inpainting and its interplay with numerical methods. We have seen that devising methods that attempt to preserve continuous properties such as the localization of the Dirichlet boundary’s influence on coarser levels pays off. We have also observed the relationship between mask density, multilevel, and multigrid methods. The latter are able to achieve much lower runtimes

for low densities, since the basis functions at low densities are inherently smoother. Finally, we noted that the widely used stopping criterion based on the relative residual can be highly misleading, especially in the context of image processing while using different classes of solvers.

In our ongoing research, we are working on extending our domain decomposition approach to more sophisticated inpainting operators, such as anisotropic nonlinear diffusion. It has been shown that those can offer an improved reconstruction quality compared to the simple homogeneous diffusion inpainting. In the companion paper to this one we tackle one of the main challenges in the encoding phase: data optimization.

## REFERENCES

- [1] T. ACAR AND M. GÖKMEN, *Image coding using weak membrane model of images*, in Visual Communications and Image Processing '94, A. K. Katsaggelos, ed., vol. 2308 of Proceedings of SPIE, SPIE Press, Bellingham, 1994, pp. 1221–1230.
- [2] S. ANDRIS, P. PETER, R. M. KAJA MOHIDEEN, J. WEICKERT, AND S. HOFFMANN, *Inpainting-based video compression in FullHD*, in Scale Space and Variational Methods in Computer Vision, A. Elmoataz, J. Fadili, Y. Quéau, J. Rabin, and L. Simon, eds., vol. 12679 of Lecture Notes in Computer Science, Springer, Cham, 2021, pp. 425–436.
- [3] S. ANDRIS, P. PETER, AND J. WEICKERT, *A proof-of-concept framework for PDE-based video compression*, in Proc. 32nd Picture Coding Symposium, Nuremberg, Germany, Dec. 2016.
- [4] M. AUGUSTIN, J. WEICKERT, AND S. ANDRIS, *Pseudodifferential inpainting: The missing link between PDE- and RBF-based interpolation*, in Scale Space and Variational Methods in Computer Vision, J. Lellmann, M. Burger, and J. Modersitzki, eds., vol. 11603 of Lecture Notes in Computer Science, Springer, Cham, 2019, pp. 67–78.
- [5] J. AUJOL, S. LADJAL, AND S. MASNOU, *Exemplar-based inpainting from a variational point of view*, SIAM Journal on Applied Mathematics, 42 (2010), pp. 1246–1285.
- [6] V. BASTANI, M. HELFROUSH, AND K. KASIRI, *Image compression based on spatial redundancy removal and image inpainting*, Journal of Zhejiang University – Science C (Computers & Electronics), 11 (2010), pp. 92–100.
- [7] Z. BELHACHMI, D. BUCUR, B. BURGETH, AND J. WEICKERT, *How to choose interpolation data in images*, SIAM Journal on Applied Mathematics, 70 (2009), pp. 333–352.
- [8] J. BERGER AND G. T. LASHER, *The use of discrete Green's functions in the numerical solution of Poisson's equation*, Illinois Journal of Mathematics, 2 (1958), pp. 593–607.
- [9] M. BERTALMIÓ, G. SAPIRO, V. CASELLES, AND C. BALLESTER, *Image inpainting*, in Proc. SIGGRAPH 2000, New Orleans, LA, July 2000, pp. 417–424.
- [10] S. BONETTINI, I. LORIS, F. PORTA, M. PRATO, AND S. REBEGOLDI, *On the convergence of a linesearch based proximal-gradient method for nonconvex optimization*, Inverse Problems, 33 (2017), Article 055005.
- [11] F. BORNEMANN AND P. DEUFLHARD, *The cascadic multigrid method for elliptic problems*, Numerische Mathematik, 75 (1996), pp. 135–152.
- [12] A. BRANDT, *Multi-level adaptive solutions to boundary-value problems*, Mathematics of Computation, 31 (1977), pp. 333–390.
- [13] M. BREUSS, L. HOELTGEN, AND G. RADOW, *Towards PDE-based video compression with optimal masks prolonged by optic flow*, Journal of Mathematical Imaging and Vision, 63 (2021), pp. 144–156.
- [14] W. L. BRIGGS, V. E. HENSON, AND S. F. MCCORMICK, *A Multigrid Tutorial*, SIAM, Philadelphia, second ed., 2000.
- [15] X.-C. CAI AND M. SARKIS, *A restricted additive Schwarz preconditioner for general sparse linear systems*, SIAM Journal on Scientific Computing, 21 (1999), pp. 792–797.
- [16] S. CARLSSON, *Sketch based coding of grey level images*, Signal Processing, 15 (1988), pp. 57–83.
- [17] R. CHEN, J. HUANG, AND X.-C. CAI, *A parallel domain decomposition algorithm for large scale image denoising*, Inverse Problems and Imaging, 13 (2019), pp. 1259–1282.

- [18] Y. CHEN, R. RANFTL, AND T. POCK, *A bi-level view of inpainting-based image compression*, in Proc. 19th Computer Vision Winter Workshop, Z. Kúkelová and J. Heller, eds., Křtiny, Czech Republic, Feb. 2014, pp. 19–25.
- [19] V. CHIZHOV AND J. WEICKERT, *Efficient data optimisation for harmonic inpainting with finite elements*, in Computer Analysis of Images and Patterns, N. Tsapatsoulis, A. Panayides, T. Theo, A. Lanitis, C. Pattichis, and M. Vento, eds., vol. 13053 of Lecture Notes in Computer Science, Springer, Cham, 2021, pp. 432–441.
- [20] F. CHUNG AND S. YAU, *Discrete Green's functions*, Journal of Combinatorial Theory, Series A, 91 (2000), p. 191–214.
- [21] U. Y. DESAI, M. M. MIZUKI, I. MASAKI, AND B. K. P. HORN, *Edge and mean based image compression*, Tech. Report 1584 (A.I. Memo), Artificial Intelligence Lab., Massachusetts Institute of Technology, Cambridge, MA, Nov. 1996.
- [22] V. DOLEAN, P. JOLIVET, AND F. NATAF, *An Introduction to Domain Decomposition Methods: Algorithms, Theory, and Parallel Implementation*, SIAM, Philadelphia, 2015.
- [23] A. A. EFROS AND T. LEUNG, *Texture synthesis by non-parametric sampling*, in Proc. Seventh International Conference on Computer Vision, vol. 2, Kerkyra, Greece, Sept. 1999, IEEE Computer Society Press, pp. 1033–1038.
- [24] E. EFSTATHIOU AND M. J. GANDER, *Why restricted additive Schwarz converges faster than additive Schwarz*, BIT Numerical Mathematics, 43 (2003), pp. 945–959.
- [25] I. GALIĆ, J. WEICKERT, M. WELK, A. BRUHN, A. BELYAEV, AND H.-P. SEIDEL, *Towards PDE-based image compression*, in Variational, Geometric and Level-Set Methods in Computer Vision, N. Paragios, O. Faugeras, T. Chan, and C. Schnörr, eds., vol. 3752 of Lecture Notes in Computer Science, Springer, Berlin, 2005, pp. 37–48.
- [26] I. GALIĆ, J. WEICKERT, M. WELK, A. BRUHN, A. BELYAEV, AND H.-P. SEIDEL, *Image compression with anisotropic diffusion*, Journal of Mathematical Imaging and Vision, 31 (2008), pp. 255–269.
- [27] M. J. GANDER, *Schwarz methods over the course of time*, Electronic Transactions on Numerical Analysis, 31 (2008), pp. 228–255.
- [28] J. GAUTIER, O. LE MEUR, AND C. GUILLEMOT, *Efficient depth map compression based on lossless edge coding and diffusion*, in Proc. 2012 Picture Coding Symposium, Kraków, Poland, May 2012, pp. 81–84.
- [29] L. GREENGARD AND V. ROKHLIN, *A fast algorithm for particle simulations*, Journal of Computational Physics, 73 (1987), pp. 325–348.
- [30] C. GUILLEMOT AND O. LE MEUR, *Image inpainting: Overview and recent advances*, IEEE Signal Processing Magazine, 31 (2014), pp. 127–144.
- [31] W. HACKBUSCH, *Multigrid Methods and Applications*, Springer, New York, 1985.
- [32] M. HESTENES AND E. STIEFEL, *Method of conjugate gradients for solving linear systems*, Journal of Research of the National Bureau of Standards, 49 (1951), p. 409–438.
- [33] L. HOELTGEN, S. SETZER, AND J. WEICKERT, *An optimal control approach to find sparse data for Laplace interpolation*, in Energy Minimisation Methods in Computer Vision and Pattern Recognition, A. Heyden, F. Kahl, C. Olsson, M. Oskarsson, and X.-C. Tai, eds., vol. 8081 of Lecture Notes in Computer Science, Springer, Berlin, 2013, pp. 151–164.
- [34] S. HOFFMANN, M. MAINBERGER, J. WEICKERT, AND M. PUHL, *Compression of depth maps with segment-based homogeneous diffusion*, in Scale Space and Variational Methods in Computer Vision, A. Kuijper, K. Bredies, T. Pock, and H. Bischof, eds., vol. 7893 of Lecture Notes in Computer Science, Springer, Berlin, 2013, pp. 319–330.
- [35] S. HOFFMANN, G. PLONKA, AND J. WEICKERT, *Discrete Green's functions for harmonic and biharmonic inpainting with sparse atoms*, in Energy Minimization Methods in Computer Vision and Pattern Recognition, X.-C. Tai, E. Bae, T. F. Chan, and M. Lysaker, eds., vol. 8932 of Lecture Notes in Computer Science, Springer, Berlin, 2015, pp. 169–182.
- [36] T. IJIMA, *Basic theory on normalization of pattern (in case of typical one-dimensional pattern)*, Bulletin of the Electrotechnical Laboratory, 26 (1962), pp. 368–388. In Japanese.
- [37] F. JOST, P. PETER, AND J. WEICKERT, *Compressing flow fields with edge-aware homogeneous diffusion inpainting*, in Proc. 45th International Conference on Acoustics, Speech, and Signal Processing (ICASSP), Barcelona, Spain, May 2020, IEEE Computer Society Press, pp. 2198–2202.

- [38] F. JOST, P. PETER, AND J. WEICKERT, *Compressing piecewise smooth images with the Mumford-Shah cartoon model*, in Proc. 28th European Signal Processing Conference (EUSIPCO), Amsterdam, Netherlands, Jan. 2021, pp. 511–515.
- [39] I. JUMAKULYYEV AND T. SCHULTZ, *Combining image space and q-space PDEs for lossless compression of diffusion MR images*, Journal of Mathematical Imaging and Vision, 65 (2023), pp. 644–656.
- [40] E. KALMOUN AND M. NASSER, *Harmonic image inpainting using the charge simulation method*, Pattern Analysis and Applications, 25 (2022), pp. 795–806.
- [41] N. KÄMPER, V. CHIZHOV, AND J. WEICKERT, *Efficient parallel algorithms for inpainting-based representations of 4K images - part II: Spatial and tonal data optimization*, Jan. 2024.
- [42] N. KÄMPER AND J. WEICKERT, *Domain decomposition algorithms for real-time homogeneous diffusion inpainting in 4K*, in Proc. 47th International Conference on Acoustics, Speech, and Signal Processing (ICASSP), Singapore, May 2022, IEEE Computer Society Press, pp. 1680–1684.
- [43] M. KATSURADA, *A mathematical study of the charge simulation method by use of peripheral conformal mappings*, Memoirs of the Institute of Science and Technology, Meiji University, 38 (1998), p. 195–212.
- [44] T. KOHLBERGER, *Variational domain decomposition for parallel image processing*, PhD thesis, University of Mannheim, Germany, 2007.
- [45] T. KOHLBERGER, C. SCHNÖRR, A. BRUHN, AND J. WEICKERT, *Domain decomposition for variational optical flow computation*, IEEE Transactions on Image Processing, 14 (2005), pp. 1125–1137.
- [46] H. KÖSTLER, M. STÜRMER, C. FREUNDL, AND U. RÜDE, *PDE based video compression in real time*, Tech. Report 07-11, Lehrstuhl für Informatik 10, Univ. Erlangen–Nürnberg, Germany, 2007.
- [47] V. KUPRADZE AND M. ALEKSIDZE, *The method of functional equations for the approximate solution of certain boundary value problems*, USSR Computational Mathematics and Mathematical Physics, 4 (1964), pp. 82–126.
- [48] Y. LI, M. SJOSTROM, U. JENNEHAG, AND R. OLSSON, *A scalable coding approach for high quality depth image compression*, in Proc. 3DTV-Conference: The True Vision – Capture, Transmission and Display of 3D Video, Zurich, Switzerland, Oct. 2012.
- [49] D. LIU, X. SUN, F. WU, S. LI, AND Y.-Q. ZHANG, *Image compression with edge-based inpainting*, IEEE Transactions on Circuits, Systems and Video Technology, 17 (2007), pp. 1273–1286.
- [50] M. MAINBERGER, A. BRUHN, J. WEICKERT, AND S. FORCHHAMMER, *Edge-based compression of cartoon-like images with homogeneous diffusion*, Pattern Recognition, 44 (2011), pp. 1859–1873.
- [51] M. MAINBERGER, S. HOFFMANN, J. WEICKERT, C. H. TANG, D. JOHANNSEN, F. NEUMANN, AND B. DOERR, *Optimising spatial and tonal data for homogeneous diffusion inpainting*, in Scale Space and Variational Methods in Computer Vision, A. M. Bruckstein, B. ter Haar Romeny, A. M. Bronstein, and M. M. Bronstein, eds., vol. 6667 of Lecture Notes in Computer Science, Springer, Berlin, 2012, pp. 26–37.
- [52] S. MASNOU AND J.-M. MOREL, *Level lines based disocclusion*, in Proc. 1998 IEEE International Conference on Image Processing, vol. 3, Chicago, IL, Oct. 1998, pp. 259–263.
- [53] A. MCADAMS, E. SIFAKIS, AND J. TERAN, *A parallel multigrid Poisson solver for fluids simulation on large grids*, in Proceedings of the 2010 ACM SIGGRAPH/Eurographics Symposium on Computer Animation, SCA '10, Goslar, Germany, 2010, Eurographics Association, p. 65–74.
- [54] K. W. MORTON AND L. M. MAYERS, *Numerical Solution of Partial Differential Equations*, Cambridge University Press, Cambridge, UK, second ed., 2005.
- [55] W. B. PENNEBAKER AND J. L. MITCHELL, *JPEG: Still Image Data Compression Standard*, Springer, New York, 1992.
- [56] P. PETER, S. HOFFMANN, F. NEDWED, L. HOELTGEN, AND J. WEICKERT, *Evaluating the true potential of diffusion-based inpainting in a compression context*, Signal Processing: Image Communication, 46 (2016), pp. 40–53.
- [57] P. PETER, L. KAUFHOLD, AND J. WEICKERT, *Turning diffusion-based image colorization into efficient color compression*, IEEE Transactions on Image Processing, 26 (2017), pp. 860–869.
- [58] P. PETER, C. SCHMALTZ, N. MACH, M. MAINBERGER, AND J. WEICKERT, *Beyond pure quality: Progressive mode, region of interest coding and real time video decoding in PDE-based image compression*, Journal of Visual Communication and Image Representation, 31 (2015), pp. 256–265.
- [59] J. RASCH, J. PFAFF, M. SCHÄFER, A. HENKEL, H. SCHWARZ, D. MARPE, AND T. WIEGAND, *A signal adaptive diffusion filter for video coding: Mathematical framework and complexity reductions*, Signal

- Processing: Image Communication, 85 (2020), Article 115861.
- [60] Y. SAAD, *Iterative Methods for Sparse Linear Systems*, SIAM, Philadelphia, second ed., 2003.
  - [61] J. SCHMALFUSS, E. SCHEURER, H. ZHAO, N. KARANTZAS, A. BRUHN, AND D. LABATE, *Blind image inpainting with sparse directional filter dictionaries for lightweight CNNs*, *Journal of Mathematical Imaging and Vision*, 65 (2023), pp. 323–339.
  - [62] C. SCHMALTZ, P. PETER, M. MAINBERGER, F. EBEL, J. WEICKERT, AND A. BRUHN, *Understanding, optimising, and extending data compression with anisotropic diffusion*, *International Journal of Computer Vision*, 108 (2014), pp. 222–240.
  - [63] C.-B. SCHÖNLIEB, *Partial Differential Equation Methods for Image Inpainting*, Cambridge Monographs on Applied and Computational Mathematics, Cambridge University Press, 2015.
  - [64] A. SOLÉ, V. CASELLES, G. SAPIRO, AND F. ARANDIGA, *Morse description and geometric encoding of digital elevation maps*, *IEEE Transactions on Image Processing*, 13 (2004), pp. 1245–1262.
  - [65] A. ST-CYR, M. J. GANDER, AND S. J. THOMAS, *Optimized multiplicative, additive, and restricted additive Schwarz preconditioning*, *SIAM Journal on Scientific Computing*, 29 (2007), pp. 2402–2425.
  - [66] G. J. SULLIVAN, J.-R. OHM, W.-J. HAN, AND T. WIEGAND, *Overview of the high efficiency video coding (HEVC) standard*, *IEEE Transactions on Circuits, Systems and Video Technology*, 22 (2012), pp. 1649–1668.
  - [67] D. S. TAUBMAN AND M. W. MARCELLIN, *JPEG 2000: Image Compression Fundamentals, Standards and Practice*, Kluwer, Boston, 2002.
  - [68] A. TOSELLI AND O. WIDLUND, *Domain Decomposition Methods - Algorithms and Theory*, vol. 34 of Springer Series in Computational Mathematics, Springer, Berlin, Heidelberg, 2005.
  - [69] U. TROTTEBERG, C. OOSTERLEE, AND A. SCHÜLLER, *Multigrid*, Academic Press, San Diego, 2001.
  - [70] J. WEICKERT, S. GREWENIG, C. SCHROERS, AND A. BRUHN, *Cyclic schemes for PDE-based image analysis*, *International Journal of Computer Vision*, 118 (2016), pp. 275–299.
  - [71] P. WESSELING, *An Introduction to Multigrid Methods*, R. T. Edwards, Flourtown, 2004.
  - [72] Y. WU, H. ZHANG, Y. SUN, AND H. GUO, *Two image compression schemes based on image inpainting*, in Proc. 2009 International Joint Conference on Computational Sciences and Optimization, Sanya, China, Apr. 2009, IEEE Computer Society Press, pp. 816–820.
  - [73] Z. XIONG, X. SUN, AND F. WU, *Block-based image compression with parameter-assistant inpainting*, *IEEE Transactions on Image Processing*, 19 (2010), pp. 1651–1657.
  - [74] J. XU, H. CHANG, AND J. QIN, *Domain decomposition method for image deblurring*, *Journal of Computational and Applied Mathematics*, 271 (2014), pp. 401–414.
  - [75] J. XU, X.-C. TAI, AND L.-L. WANG, *A two-level domain decomposition method for image restoration*, *Inverse Problems and Imaging*, 4 (2010), pp. 523–545.
  - [76] C. ZHAO AND M. DU, *Image compression based on PDEs*, in Proc. 2011 International Conference of Computer Science and Network Technology, Harbin, China, Dec. 2011, pp. 1768–1771.